High-resolution X-Ray spectral diagnostics of Active Galactic Nuclei

Steenbrugge, K.C.

Chapter 2

Instrumentation and statistical analysis

It has only been possible to obtain high resolution X-ray spectra of Active Galactic Nuclei since the launch of XMM-*Newton* and *Chandra*. The different instruments onboard each spacecraft provide complementary spectra. In this thesis we present spectra of NGC 5548, NGC 4593, IC 4329A and Ton 1388 taken with the grating spectrometers onboard XMM-*Newton* as well as the different grating spectrometers on *Chandra*. High resolution X-ray spectra of AGN are still photon limited, the statistical analysis methods used in this thesis will be briefly described at the end of this Chapter.

2.1 XMM-*Newton*

The XMM-*Newton* satellite has six instruments onboard and three X-ray telescopes. All instruments can observe simultaneously. An overview of the XMM-*Newton* satellite is shown in Fig. 2.1. Five of the instruments are X-ray instruments, the sixth is the optical monitor. The three European Photon Imaging Camera (EPIC) instruments contain CCDs with moderate spectral resolution, while the two Reflection Grating Spectrometers are dispersive instruments and have high spectral resolution.

The EPIC instruments are high-throughput, medium angular resolution ($\sim$ 15 arcsec half energy width) X-ray telescopes, which have a CCD camera at the focal plane. The CCDs have an energy resolution between 50 eV and 185 eV, allowing for non-dispersive spectroscopy. The peak effective area is 0.15 m^2 at 1 keV and 0.05 m^2 at 5 keV. The instruments are sensitive up to energies of about 15 keV. The EPIC in-

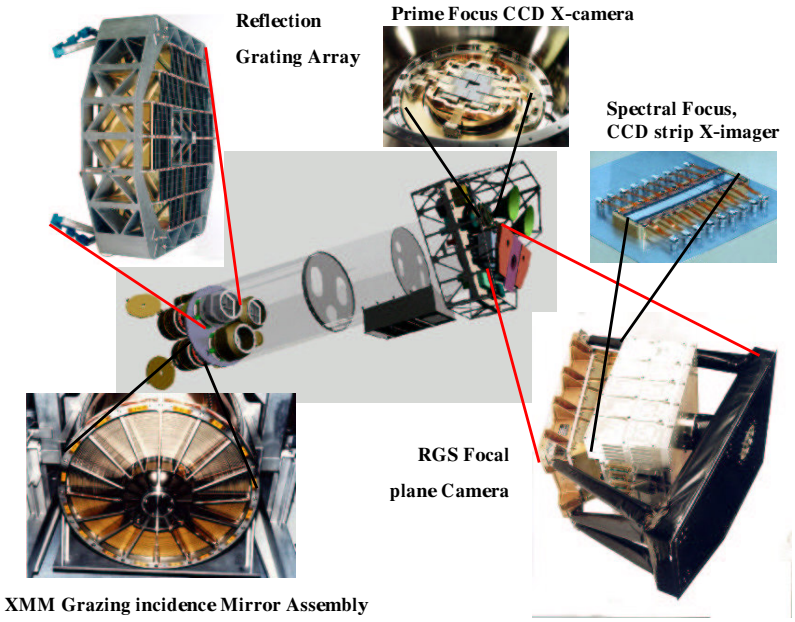

Figure 2.1: An overview of the different instruments onboard XMM-*Newton*. An advantage is that all instruments can observe simultaneously, covering a energy band between 0.2 and 15 keV (Courtesy of J. A. M. Bleeker).

struments consist of the pn-junction device (Strüder et al. 2001) which has an energy resolution ranging between 90 eV at 1 keV and 185 eV at 10 keV (XMM-*Newton* Users' Handbook) and the metal oxide semiconductors MOS 1 and MOS 2 (Turner et al. 2001). Each MOS camera shares a telescope with an RGS grating device. About half of the incoming X-rays are deflected toward the Reflection Grating Spectrometers, while 44 % of the incoming X-rays pass undeflected and are detected by the MOS cameras. As a result the throughput for each MOS instrument is about half that for the pn. The energy resolution of the MOS cameras ranges between 50 eV at 0.4 keV to 180 eV at 10 keV (XMM-*Newton* Users' Handbook). In this thesis the EPIC spectra were mainly used for determining the continuum, the broadened soft X-ray emission lines and fitting the Fe Kα emission line at 6.4 keV.

There are two high spectral resolution instruments, the Reflection Grating Spec-

trometers RGS 1 and RGS 2 (den Herder et al. 2001). These have a relatively large effective area of 0.09 m^2 at 24 Å (see Fig 2.4). The wavelength resolution is better or equal to 0.07 Å for first order spectra, and is 0.04 Å for second order spectra (XMM-*Newton* Users' Handbook). The uncertainty in absolute wavelength scale is 8 mÅ (den Herder et al. 2001). The instruments are sensitive between 5 and 38 Å, however, the calibration below 7 Å is still uncertain. Due to a failure of two CCD chains shortly after launch, there is a data gap between $10 - 14$ Å for RGS 1 and between $20 - 24$ Å for RGS 2. Fig. 2.2 shows the pn and RGS spectra of IC 4329A, illustrating the differences between both instruments. In this wavelength band oxygen, nitrogen, carbon and iron have strong absorption lines. Iron transitions from the lowly ionized Fe VI to highly ionized Fe XXIV are detectable in this wavelength band. In principle one can determine the ionization stage of the observed gas using only iron ions, and thus avoid having uncertainties due to unknown abundances of the other ions. The high resolution spectra from the RGS instruments are extensively used in this thesis. The only XMM-*Newton* instrument that was not extensively used in this thesis is the Optical Monitor

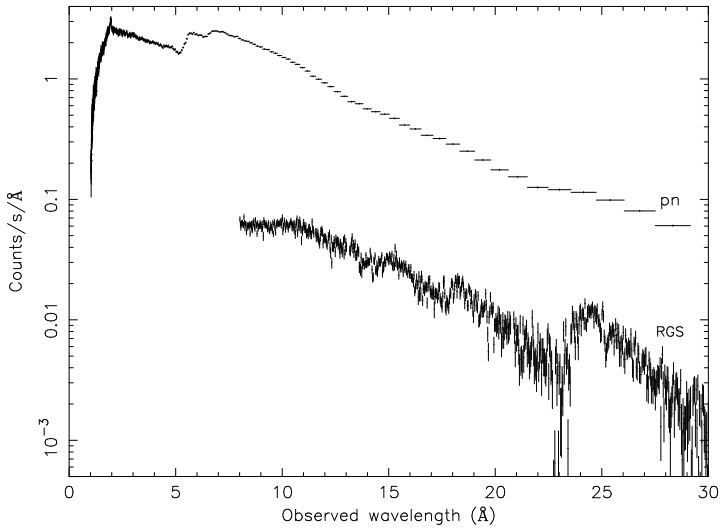

Figure 2.2: The pn and RGS spectrum of the heavily absorbed Seyfert 1 galaxy IC 4329A. RGS 1 and RGS 2 were averaged for clarity. The RGS data between 5 and 7 Å are not included due to calibration uncertainties. Note the difference in count rate as well as the difference in spectral resolution.

(OM). With this instrument optical and UV spectra and images can be obtained.

2.2 *Chandra*

For the current dispersive X-ray instruments the effective spectral resolution is a function of the size of the observed object. The AGN studied in this thesis are point sources in the X-ray band, as a result all high spectral resolution instruments onboard of both observatories can be used without loss of spectral resolution. The *Chandra* observatory has several instruments, which however cannot observe simultaneously as there is only one X-ray telescope. There are four cameras onboard: the Advanced CCD Imaging Spectrometer-S (ACIS-S) which is sensitive between 1 and 60 Å, the High Resolution Camera-S (HRC-S) which is sensitive between 1 and 180 Å, the Advanced CCD Imaging Spectrometer-I (ACIS-I) detector which is optimized for imaging, and the High Resolution Camera-I (HRC-I), which has the highest spatial resolution. The ACIS-I has a spatial resolution of 0.1 arcsec, but the High Resolution Mirror Assembly (HRMA) has a spatial point spread function of 0.5 arcsec, but the spectral resolution is similar to the EPIC instruments on XMM-*Newton* (Chandra at a Glance, http://cxc.harvard.edu/cdo/about_chandra/). This instrument and the HRC-I are not used in this thesis. In Fig. 2.3 the X-ray focusing mirror onboard *Chandra* is shown.

There are three grating arrays onboard: the Low Energy Transmission Grating (LETG), the High Energy Grating (HEG) and the Medium Energy Grating (MEG). The latter two gratings are operated simultaneously and are collectively called the High Energy Transmission Grating (HETG). Details of the characteristics of these three different gratings are listed in Table 2.1. The effective area of these instruments is significantly below that of the RGS instruments, except for wavelengths below 11 Å (see Fig 2.4).

The HEG is the grating with the highest resolution and was mainly used to study the Fe Kα emission line and the highly ionized absorber. The MEG has a lower resolution, but can be used to study also the less ionized gas. These grating instruments are usually used in combination with the ACIS-S detector. The LETG has the longest wavelength coverage of all high spectral resolution X-ray instruments, allowing study of the soft excess in AGN and the complete ionization range of the warm absorber. The LETG is in general used in combination with the HRC-S detector; this instrumental set-up is called LETGS. For all the spectrometers the spectral resolution is a constant as function of wavelength. Thus the velocity resolution of the LETG for wavelengths longer than 33.74 Å (C VI Lyα) is better than the velocity resolution of the MEG below 15.2 Å. For the LETGS, spectral order separation is not possible, and thus the higher order spectra need to be modeled during the analysis.

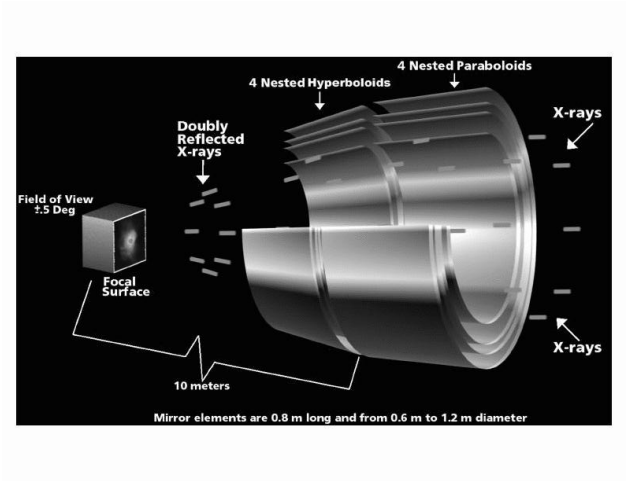

Figure 2.3: The X-ray focusing mirror of the *Chandra* telescope. This telescope is very similar to the one used on XMM-*Newton* (from http:chandra.harvard.edu/resources/illustrations/teleSchemGraz3D.html).

2.3 Comparison between observatories

The main advantage of the XMM-*Newton* observatory is the fact that all instruments observe simultaneously. This allows for an accurate continuum modeling as well as

Table 2.1: Comparison between the different spectrometers on *Chandra*. Data were taken from the Chandra calibration website. For comparison the values for the RGS are also given (from the XMM-Newton Users' Handbook).

Instr.	wavelength band	resolution (FWHM)	absolute wavelength scale
HEG	1.5 – 15 Å	0.012 Å	6 mÅ
MEG	1.5 – 31 Å	0.023 Å	11 mÅ
LETG	1.5 – 170 Å	0.05 Å	13 mÅ
RGS	5 – 38 Å	0.07 Å	8 mÅ

studying the spectral diagnostics of the source. This is especially important in the debate about relativistically broadened soft X-ray emission lines and the study of other broadened emission lines. Another advantage is the large effective area of the RGS instruments, allowing to study possible spectral variability in more sources and on shorter timescales than possible with *Chandra* spectrometers. Fig. 2.4 shows a comparison in effective area for the different high spectral resolution instruments.

An advantage of the *Chandra* instruments is the higher spectral resolution, allowing in some cases to resolve some velocity components. The LETGS has a large wavelength band, as a result L-shell lines from silicon, sulfur, neon, and other, less abundant elements are observed. In general, the RGS instruments are well suited to study heavily absorbed (due to Galactic or intrinsic absorption) AGN. Longer wavelengths are more affected by absorption than shorter wavelengths, thus relatively bright AGN with low Galactic or intrinsic absorption are optimally studied with the LETGS. The HETG is useful if the highest spectral resolution is required, for instance to disentangle outflow velocity components. Another advantage is that the *Chandra* observatory dithers, smoothing out any hot pixels and CCD-gaps. This is not (yet) the case for the XMM-*Newton* observatory.

2.4 Statistical analysis

In general the high resolution spectra of AGN are photon limited. As a result, the spectra which have exposure times less than 100 ks for RGS and HETG and less than 200 ks for the LETGS can be rather noisy. It is thus important that in the spectral analysis noise and real spectral features are separated. In fitting absorption lines we reduce the effects of noise by using self consistent models for all absorption features of each ion. As Seyfert 1 galaxies have an absorption dominated spectrum, the need for self-consistent emission line fitting is relatively small. The number of narrow emission lines in most AGN is in general very small (the O VII forbidden line and a few others). The absorber is photoionized, and all photoionization models used in this thesis assume that the absorber is a geometrically thin slab, with negligible (re)-emission from the slab itself. In the simplest case we fit the absorption lines and continuum absorption edges from a certain ion simultaneously. As the oscillator strengths and continuum opacities for the different lines and edges of the same ion are known and held fixed, this improves the stability of the fit. However, for those ions where continuum or edge absorption dominates over the wavelength range that is covered, this is not a stringent method. Weak continuum absorption features can be easily confused with any mismatch in the continuum emission model or remaining calibration uncertainties.

A more stringent method is to use a photoionization code to couple the different

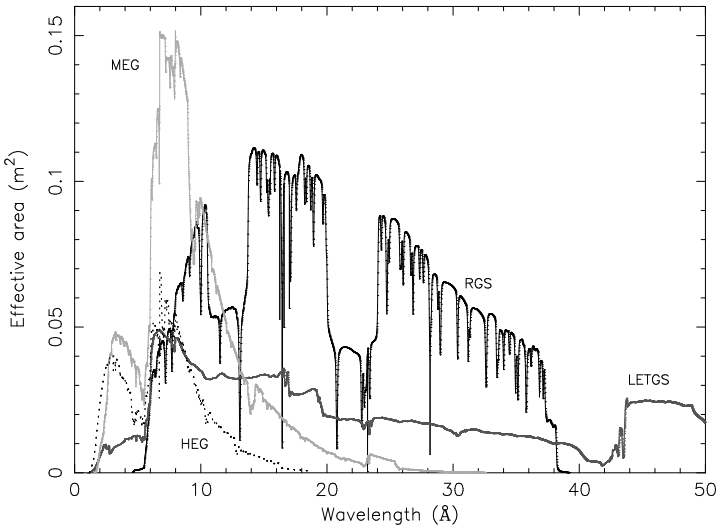

Figure 2.4: Comparison of the effective areas for the different high resolution spectrometers as a function of wavelength. For RGS 1 and RGS 2 we took the effective are from the IC 4329A data set and added RGS 1 and RGS 2 for clarity. For the LETGS, MEG and HEG (in combination with the ACIS-S) we took the effective area from the *Chandra* 2002 data on NGC 5548. For LETGS we added the effective area of the first 10 spectral orders.

ions. In this method only the ionization parameter, the total column density, the elemental abundances, the outflow velocity and velocity broadening are free parameters. With this method there are tens, and often hundreds of absorption lines fitted. This in general leads to high statistical significance of an absorption component, even if most individual lines are only detected with 1 or 2 σ significance. In this case the continuum and edge absorption is also self-consistently taken into account, even for ions with weak continuum absorption. However, there is a caveat: there are uncertainties in the photoionization codes, which result in systematic uncertainties in the analysis. These uncertainties are hard to quantify. Further, in most cases at least three such absorption components are necessary to fit the spectra, increasing the uncertainties, as the total column densities and the different ionization parameters are correlated parameters.

In a final method we force the distribution of the column density versus ionization parameter to be a power-law, leaving only the slope, the normalization, the elemen-

tal abundances, the outflow velocity and velocity broadening free parameters. If the assumption of a power-law distribution is correct, then this model should fit all the absorption lines and edges in the spectrum. Thus we need only one component, reducing the numbers of free parameters in the fit. However, here again any possible uncertainties in the photoionization code results in systematic uncertainties. Also, we do make an a priori assumption about the ionization structure which need not be correct.

We can derive accurate spectral diagnostics for the warm absorber with the above methods, even if the spectrum is rather noisy.

For the quasar Ton 1388, we do not detect a warm absorber, but only a few weak absorption lines. Toward this source there are 16 known Lyα absorbers detected in the optical and UV bands. We thus assumed that these absorption lines were associated with one or more known Lyα absorber. It is presumed that a large fraction of the local baryons are hot and form the Warm-Hot Intergalactic Medium (WHIM; Cen & Ostriker 1999). As these absorption lines are probably unrelated to the quasar, we can only fit ion per ion, either assuming photoionization or collisional ionization. As the absorption lines in the spectrum are weak, we allowed only identifications with X-ray absorption lines with high oscillator strengths and froze the redshift to one where in the UV band a Lyα absorber has been detected. With this method we tried to reduce the chances of fitting noise. Again, we tried to fit the absorption lines self consistently, namely if an ion of a certain ionization parameter is observed, then we try to ascertain whether or not we also see other ions with similar ionization parameter or temperature.

A similar situation occurs for the absorption lines at zero redshift detected in nearly all the spectra presented in this thesis. In general we only mention them briefly and quote an equivalent width as there are only one or two lines detected. However, from the fact that they occur in the different spectra we can conclude that they are real.

References

Cen, R. & Ostriker, J. P., 1999, ApJ, 514, 1

Chandra at a Glance, http://cxc.harvard.edu/cdo/about_chandra/

den Herder, J. W., Brinkman, A. C., Kahn, S. M. et al., 2001, A&A, 365, L7

Ehle, M., Breitfellner, M., González Riestra, R., et al., 2004, XMM-Newton Users' Handbook, version 2.2

Kaastra, J. S., Steenbrugge, K. C., Raassen, A. J. J., et al., 2002, A&A, 386, 427

Strüder, L., Briel, U. G., Dennerl, K., et al., 2001, A&A, 365, L18

Turner, M. J. L., Abbey, A., Arnaud, M., et al., 2001, A&A, 365, L27